Suppressing qubit dephasing using real-time Hamiltonian estimation

M. D. Shulman,[1] S. P. Harvey,[1] J. M. Nichol,[1] S. D. Bartlett,[2] A. C. Doherty,[2] V. Umansky,[3] and A. Yacoby[1]

[1] *Department of Physics, Harvard University, Cambridge, MA, 02138, USA*
[2] *Centre for Engineered Quantum Systems, School of Physics, The University of Sydney, Sydney, NSW 2006, Australia*
[3] *Braun Center for Submicron Research, Department of Condensed Matter Physics, Weizmann Institute of Science, Rehovot 76100 Israel*

(Dated: May 5, 2014)

Unwanted interaction between a quantum system and its fluctuating environment leads to decoherence and is the primary obstacle to establishing a scalable quantum information processing architecture. Strategies such as environmental [1, 2] and materials engineering [3], quantum error correction [4, 5] and dynamical decoupling [6] can mitigate decoherence, but generally increase experimental complexity. Here we improve coherence in a qubit using real-time Hamiltonian parameter estimation [7]. Using a rapidly converging Bayesian approach, we precisely measure the splitting in a singlet-triplet spin qubit faster than the surrounding nuclear bath fluctuates. We continuously adjust qubit control parameters based on this information, thereby improving the inhomogenously broadened coherence time (T_2^*) from tens of nanoseconds to above 2 μs and demonstrating the effectiveness of Hamiltonian estimation in reducing the effects of correlated noise in quantum systems. Because the technique demonstrated here is compatible with arbitrary qubit operations, it is a natural complement to quantum error correction and can be used to improve the performance of a wide variety of qubits in both metrological and quantum-information-processing applications.

Hamiltonian parameter estimation is a rich field of active experimental and theoretical research that enables precise characterization and control of quantum systems [7]. For example, magnetometry schemes employing Hamiltonian learning have demonstrated dynamic range and sensitivities exceeding those of standard methods [8, 9]. Such applications focused on estimating parameters that are quasistatic on experimental timescales. However, the effectiveness of Hamiltonian learning also offers exciting prospects for estimating fluctuating parameters responsible for decoherence in quantum systems. In this work we employ techniques from Hamiltonian estimation to prolong the coherence of a qubit by more than a factor of 30. Importantly, our estimation protocol, which is based on recent theoretical work [10], requires relatively few measurements (≈100) which we perform rapidly enough (total time $\approx 100\mu s$) to resolve the qubit splitting faster than its characteristic fluctuation time. We adopt a paradigm in which we separate experiments into "estimation" and "operation" segments, and we use information from the former to optimize control parameters for the latter in real-time. Our method dramatically prolongs coherence without using complex pulse sequences such as those required for non-identity dynamically decoupled operations [11].

The singlet-triplet (S-T_0) qubit [12, 13] studied in this work is formed by two gate-defined lateral quantum dots (QDs) in a GaAs/AlGaAs heterostructure (Fig. 1**a**) similar to that of refs. [14, 15]. The qubit can be rapidly initialized in the singlet state $|S\rangle$ in ≈ 20 ns and read out with 98% fidelity in $\approx 1\ \mu s$ [16, 17] (see SOM). Universal quantum control is provided by two distinct drives [18]: the exchange splitting, J, between $|S\rangle$ and $|T_0\rangle$, and the magnetic field gradient, ΔB_z, due to the hyperfine interaction with host Ga and As nuclei. The Bloch sphere representation for this qubit can be seen in Fig. 1**b**.

In this work, we focus on qubit evolution around ΔB_z (Fig. 2**a**). Due to statistical fluctuations of the nuclei, ΔB_z varies randomly in time, and consequently oscillations around this field gradient decay in a time $T_2^* \approx 10$ ns [12]. A nuclear feedback scheme relying on dynamic nuclear polarization [2] can be employed to set the mean gradient, ($g^*\mu_B\Delta B_z/h \approx 60$ MHz in this work) as well as reduce the variance of the fluctuations. Here, $g^* \approx -0.44$ is the effective gyromagnetic ratio in GaAs, μ_B is the Bohr magneton and h is Planck's constant. In what follows, we adopt units where $g^*\mu_B/h = 1$. With the use of this feedback, the coherence time improves to $T_2^* \approx 100$ ns [2] (Fig. 2**b**), limited by the low nuclear pumping efficiency [18]. Crucially, the residual fluctuations are considerably slower than the timescale of qubit operations [19]. To take advantage of these slow dynamics, we introduce a method that measures the fluctuations and manipulates the qubit based on precise knowledge but not precise control of the environment.

We operate the qubit in the rotating frame of ΔB_z, where qubit rotations are driven by modulating J at the frequency $\frac{\Omega_J}{2\pi} = \Delta B_z$ [20, 21]. To measure Rabi oscillations, the qubit is adiabatically prepared in the ground state of ΔB_z ($|\psi\rangle$=$|\uparrow\ \downarrow\rangle$), and an oscillating J is switched on (Fig. 2**e**), causing the qubit to precess around J in the rotating frame. Additionally, we perform a Ramsey experiment (Fig. 2**c**) to determine T_2^*, and as expected, we observe the same decay (Fig. 2**d**) as Fig. 2**b**. More precisely, the data in Fig. 2**d** represent the average of 1024 experimental repetitions of the same qubit operation sequence immediately following nuclear feedback. The feedback cycle resets ΔB_z to its mean value (60MHz)

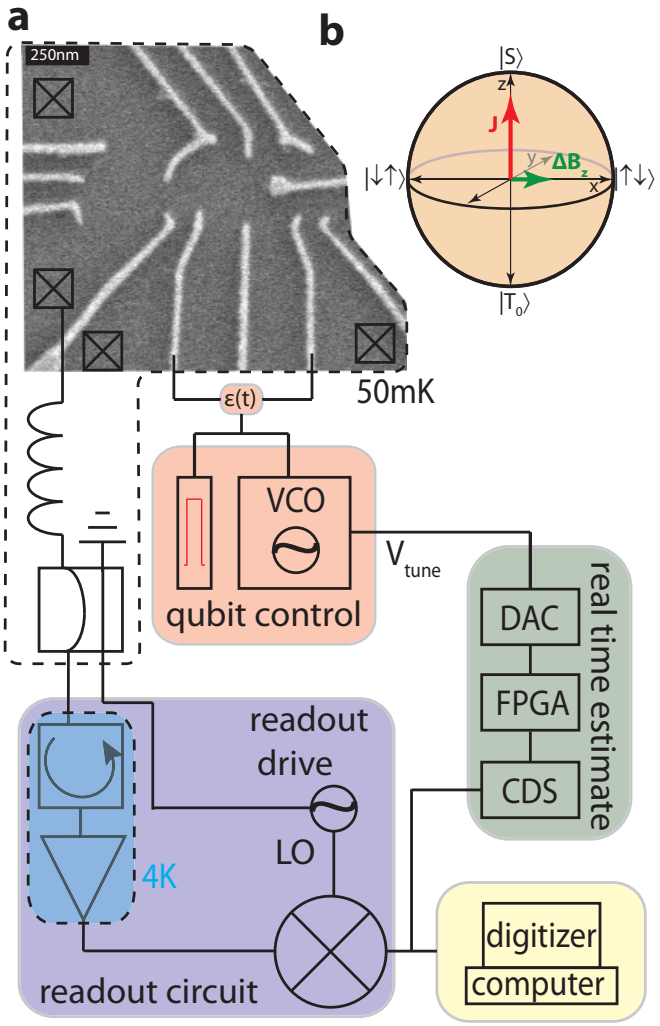

FIG. 1. Experimental apparatus. **a,** A scanning electron microscope image of the double QD with a schematic of the apparatus used for adaptive qubit control. A floating metal gate protruding from the right can be seen which increases the capacitance between the qubit and an adjacent qubit (not pictured), which is left inactive for this work. The reflected readout drive signal is demodulated to DC, digitized by a correlated double sampler (CDS), and ΔB_z is estimated in real time by the field programmable gate array (FPGA). The FPGA updates the digital to analog converter (DAC) in order to keep the voltage controlled oscillator (VCO) resonant with the estimated value of ΔB_z. The VCO controls the voltage detuning, $\epsilon(t)$ between the QDs, which, in turn, modulates J at Ω_J. **b,** The Bloch sphere representation for the S-T_0 qubit showing the two axes of control, J and ΔB_z.

with residual fluctuations of $(\sqrt{2}\pi T_2^*)^{-1} \approx 10$MHz between experimental repetitions. However, within a given experimental repetition, ΔB_z is approximately constant. Therefore we present an adaptive control scheme where, in following nuclear feedback, we quickly estimate ΔB_z and tune $\frac{\Omega_J}{2\pi} = \Delta B_z$ in order to prolong qubit coherence (Fig. 3**a**).

To estimate ΔB_z, we repeatedly perform a series of single-shot measurements after allowing it to evolve around ΔB_z for some amount of time (Fig. 2**a**). Rather than fixing this evolution time to be constant for all trials, we make use of recent theoretical results in Hamiltonian parameter estimation [10, 21, 22] and choose linearly increasing evolution times, $t_k = kt_{samp}$, where $k = 1, 2, \cdots, N$. We choose the sampling time t_{samp} such that the estimation bandwidth $\mathcal{B} = \frac{1}{2t_{samp}}$ is several times larger than the magnitude of the residual fluctuations in ΔB_z, roughly 10 MHz. With a Bayesian approach to estimate ΔB_z in real-time, the longer evolution times (large k) leverage the increased precision obtained from earlier measurements to provide improved sensitivity, allowing the estimate to outperform the standard limit associated with repeating measurements at a single evolution time. Denoting the outcome of the k^{th} measurement as m_k (either $|S\rangle$ or $|T_0\rangle$), we define $P(m_k|\Delta B_z)$ as the conditional probability for m_k given a value ΔB_z. We write

$$P(m_k|\Delta B_z) = \frac{1}{2}\left[1 + r_k\left(\alpha + \beta\cos\left(2\pi\Delta B_z t_k\right)\right)\right], \quad (1)$$

where r_k=1 (−1) for m_k=$|S\rangle$ ($|T_0\rangle$), and $\alpha = 0.25$ and $\beta = 0.67$ are parameters determined by the measurement error and axis of rotation on the Bloch sphere (see SOM). Since measurement outcomes are assumed to be independent, we write the conditional probability for ΔB_z given the results of N measurements as:

$$P(\Delta B_z|m_N, m_{N-1}, ...m_1) \quad (2)$$
$$= P(\Delta B_z|m_{N-1}, ...m_1)\cdot P(\Delta B_z|m_N) \quad (3)$$
$$= \prod_{k=1}^{N} P(\Delta B_z|m_k). \quad (4)$$

Using Bayes' rule, i.e., $P(\Delta B_z|m_k) = P(m_k|\Delta B_z)P(\Delta B_z)/P(m_k)$, and eq. 1, we can rewrite eq. 4 as:

$$P(\Delta B_z|m_N, m_{N-1}, ...m_1) =$$
$$P_0(\Delta B_z)\mathcal{N}\prod_{k=1}^{N}\left(1 + r_k\left(\alpha + \beta\cos\left(2\pi\Delta B_z t_k\right)\right)\right], \quad (5)$$

where $\mathcal{N}$ is a normalization constant and $P_0(\Delta B_z)$ is a prior distribution to which the algorithm is empirically insensitive, and which we take to be a constant over the estimation bandwidth. After the last measurement, we find the value of ΔB_z that maximizes the posterior distribution $P(\Delta B_z|m_N, m_{N-1}, ...m_1)$.

We implement this algorithm in real time on a field-programmable gate array (FPGA) for 256 linearly spaced frequencies between 50 and 70MHz. With each measurement m_k, the readout signal is digitized and passed to the FPGA, which computes the Bayesian estimate of ΔB_z and updates an analog voltage that tunes the frequency of a voltage controlled oscillator (Fig. 1**a**) (see

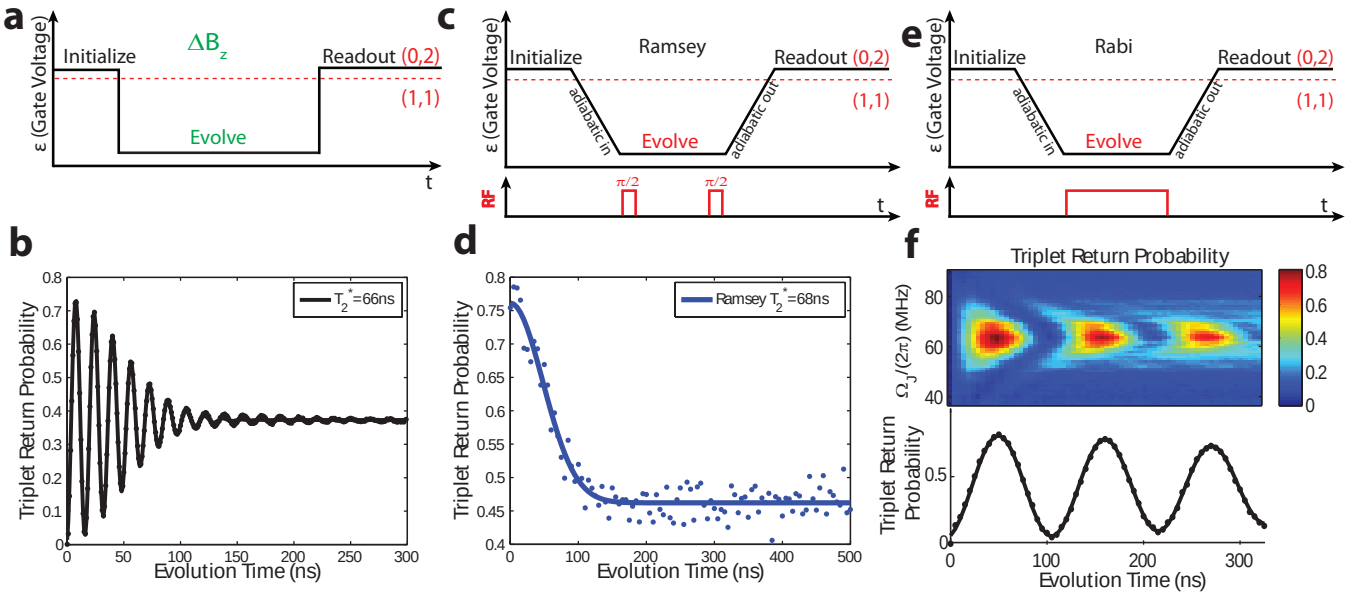

FIG. 2. ΔB_z oscillations. **a,** The pulse sequence used to estimate ΔB_z. **b,**. Using nuclear feedback, ΔB_z oscillations decay in a coherence time $T_2^* \approx 70$ns due to residual slow fluctuations in ΔB_z. **c,** The Ramsey sequence used to operate the S-T_0 qubit in the rotating frame. **d,** The Ramsey contrast decays similarly to the oscillations in **(c)** due to the same residual slow fluctuations in ΔB_z. **e,** The Rabi pulse sequence used to drive the qubit in the rotating frame. **f,** The rotating frame S-T_0 qubit exhibits the typical behavior when sweeping drive frequency and time (top). When driven on resonance (bottom), the qubit undergoes Rabi oscillations, demonstrating control in the rotating frame.

SOM). Following the N^{th} sample, $\frac{\Omega_J}{2\pi}$ nearly matches ΔB_z, and since the nuclear dynamics are slow, the qubit can be operated with long coherence without any additional complexity. To quantify how well the FPGA estimate matches ΔB_z, we perform a Ramsey experiment (deliberately detuned to observe oscillations) with this real-time tracking of ΔB_z and find optimal performance for $N \approx 120$, with a maximum experimental repetition rate, limited by the FPGA, of 250kHz and a sampling time $t_{samp} = 12$ ns. Under these conditions, we observe $T_2^* = 2066$ ns, a 30-fold increase in coherence (Fig. 3**b**). We note that these data are taken with the same pulse sequence as those in Fig. 2**d**. To further compare qubit operations with and without this technique, we measure Ramsey fringes for ≈ 250s (Fig. 3**d**), and histogram the observed Ramsey detunings. With adaptive control we observe a stark narrowing of the observed frequency distribution, consistent with this improved coherence (Fig. 3**c**).

Although the estimation scheme employed here is theoretically predicted to improve monotonically with N [10], we find that there is an optimum ($N \approx 120$), after which T_2^* slowly decreases with increasing N (Fig. 4**a**). A possible explanation for this trend is fluctuation of the nuclear gradient during the estimation period. To investigate this, we obtain time records of ΔB_z using the Bayesian estimate and find that its variance increases linearly in time at the rate of $(6.7 \pm .7\text{kHz})^2 \mu s^{-1}$ (Fig. 4**c**). The observed linear behavior suggests a model where the nuclear gradient diffuses, and using the measured diffusion of ΔB_z, we simulate the performance of the Bayesian estimate as a function of N(see SOM). Given that the simulation has no free parameters, we find good agreement with the observed T_2^*, indicating that indeed, diffusion limits the accuracy with which we can measure ΔB_z (Fig. 4**a**).

This model suggests that increasing the rate of measurements during estimation will improve the accuracy of the Bayesian estimate. Because our FPGA limits the repetition rate of qubit operations to 250 kHz, we demonstrate the effect of faster measurements through software post-processing with the same Bayesian estimate. To do so, we first use the same estimation sequence, but for the operation segment, we measure the outcome after evolving around ΔB_z for a single evolution time, t_{evo}, rather than performing a rotating frame Ramsey experiment, and we repeat this experiment a total of N_{tot} times. In processing, we perform the Bayesian estimate of each $\Delta B_{z,i}$, sort the data by adjusted time $\tau_i = \frac{\Delta B_{z,i} t_{evo,i}}{\langle \Delta B_z \rangle}$ (for $i = 1, 2, \cdots, N_{tot}$), and average together points of similar τ in order to observe oscillations (see SOM). We fit the decay of these oscillations to extract T_2^* and the precision of the Bayesian estimate, $\sigma_{\Delta B_z} = \left(\sqrt{2}\pi T_2^*\right)^{-1}$ (see SOM). For the same operation and estimation parameters, we find that T_2^* extracted from software post-

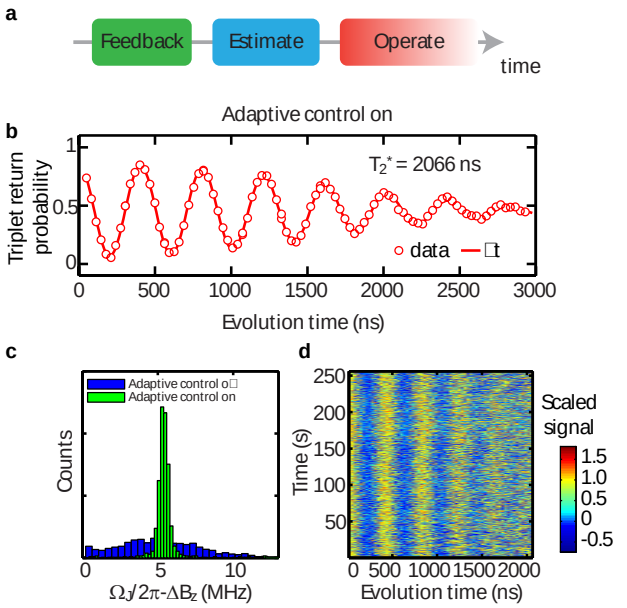

FIG. 3. Adaptive control. **a,** For these measurements we first perform our standard nuclear feedback, then quickly estimate ΔB_z and update the qubit control, then operate the qubit at the correct driving frequency. **b,** Using adaptive control, we perform a Ramsey experiment (deliberately detuned to see oscillations) and obtain coherence times larger than 2 μs. **c,** Histograms of measured Ramsey detunings with and without adaptive control. For clarity, these data were taken with a different mean detuning than those in **(b)**. **d,** Raw data for 1024 consecutive Ramsey experiments with adaptive control lasting 250 s in total. A value of 1 corresponds to $|T_0\rangle$ and 0 corresponds to $|S\rangle$. Stabilized oscillations are clearly visible in the data, demonstrating the effect of adaptive control.

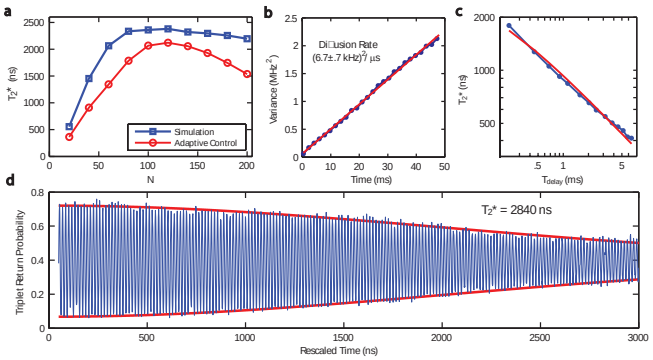

FIG. 4. ΔB_z diffusion. **a,** The coherence time, T_2^* using the adaptive control and for a simulation show a peak, indicating that there is an optimal number of measurements to make when estimating ΔB_z. **b,** When many time traces of ΔB_z are considered, their variance grows linearly with time, indicating a diffusion process. **c,** The scaling of T_2^* as a function of T_{delay} for software scaled data is consistent with diffusion of ΔB_z. **d,** The performance of the Bayesian estimate of ΔB_z can be estimated using software post processing, giving $T_2^* = 2840$ns, which corresponds to a precision of $\sigma_{\Delta B_z} = 80$kHz.

processing agrees with that extracted from adaptive control (see SOM). Using a repetition rate as high as 667kHz, we show coherence times above 2800 ns, corresponding to an error of $\sigma_{\Delta B_z}$=80kHz (Fig. 4**d**), indicating that improvements are easily attainable by using faster (commercially available) FPGAs.

Additionally, we use this post-processing technique to examine the effect of this technique on the duty cycle of experiments as well as the stability of the ΔB_z estimate. To do so we introduce a delay T_{delay} between the estimation of ΔB_z and the single evolution measurement performed in place of the operation. We find $T_2^* = (a + bT_{delay}^c)^{-0.5}$, where c = 0.99 (Fig. 4**c**), consistent with diffusion of ΔB_z. Indeed, this dependence underscores the potential of adaptive control, since it demonstrates that after a single estimation sequence, the qubit can be operated for $>$ 1ms with $T_2^* > 1\mu$s. Thus, adaptive control need not significantly reduce the experimental duty cycle.

In this work, we have used real-time adaptive control based on Hamiltonian parameter estimation of a $S - T_0$ spin qubit to prolong T_2^* from 70ns to more than 2 μs. Dephasing due to nuclear spins has long been considered a significant obstacle to quantum information processing using semiconductor spin qubits [23]. However, here we have shown that with a combination of nuclear feedback and real-time Hamiltonian estimation, we are able to achieve ratios of coherence times to operation times in excess of 200 without recourse to dynamical decoupling. If the same adaptive control techniques were applied to gradients as high as 1 GHz [18], ratios exceeding 4000 would be possible, and longer coherence times may be attainable with more sophisticated techniques [10]. The method we have presented is straightforward to implement, compatible with arbitrary qubit operations, and general to all qubits that suffer from non-Markovian noise. Looking ahead, it is likely, therefore, to play a key role in realistic quantum error correction efforts, where even modest improvements in baseline error rate greatly diminish experimental complexity and enhance prospects for a scalable quantum information processing architecture.

M.D.S, S.P.H, and J.M.N. contributed equally to this work. Correspondence should be directed to AY at yacoby@physics.harvard.edu We acknowledge James MacArthur for building the correlated double sampler. This research was funded by the United States Department of Defense, the Office of the Director of National Intelligence (ODNI), Intelligence Advanced Research Projects Activity (IARPA), and the Army Research Office grant (W911NF-11-1-0068 and W911NF-11-1-0068). All statements of fact, opinion or conclusions contained herein are those of the authors and should not be construed as representing the official views or policies either expressly or implied of of IARPA, the ODNI, or the U.S. Government. S.P.H was supported by the De-

partment of Defense (DoD) through the National Defense Science & Engineering Graduate Fellowship (NDSEG) Program. ACD acknowledges discussions with Matthew Wadrop regarding extracting diffusion constants. ACD and SDB acknowledge support from the ARC via the Centre of Excellence in Engineering Quantum Systems (EQuS) project number CE110001013. This work was performed in part at the Center for Nanoscale Systems (CNS), a member of the National Nanotechnology Infrastructure Network (NNIN), which is supported by the National Science Foundation under NSF award no. ECS-0335765. CNS is part of Harvard University.

[1] D. A. Hite, Y. Colombe, A. C. Wilson, K. R. Brown, U. Warring, R. Jördens, J. D. Jost, K. S. McKay, D. P. Pappas, D. Leibfried, and D. J. Wineland. 100-fold reduction of electric-field noise in an ion trap cleaned with *in situ* argon-ion-beam bombardment. *Phys. Rev. Lett.*, 109:103001, Sep 2012. doi: 10.1103/PhysRevLett.109.103001. URL `http://link.aps.org/doi/10.1103/PhysRevLett.109.103001`.

[2] H. Bluhm, S. Foletti, D. Mahalu, V. Umansky, and A. Yacoby. Enhancing the coherence of a spin qubit by operating it as a feedback loop that controls its nuclear spin bath. *Phys. Rev. Lett.*, 105:216803, 2010.

[3] Hanhee Paik, D. I. Schuster, Lev S. Bishop, G. Kirchmair, G. Catelani, A. P. Sears, B. R. Johnson, M. J. Reagor, L. Frunzio, L. I. Glazman, S. M. Girvin, M. H. Devoret, and R. J. Schoelkopf. Observation of high coherence in Josephson junction qubits measured in a three-dimensional circuit QED architecture. *Phys. Rev. Lett.*, 107:240501, Dec 2011. doi: 10.1103/PhysRevLett.107.240501. URL `http://link.aps.org/doi/10.1103/PhysRevLett.107.240501`.

[4] M.A. Nielsen and I.L. Chuang. *Quantum Computation and Quantum Information*. Cambridge University Press, 2000.

[5] M.D. Reed, L. DiCarlo, S.E. Nigg, L. Sun, L Frunzio, S. M. Girvin, and R. J. Schoelkopf. Realization of a three-qubit quantum error correction with superconducting circuits. *Nature*, 482:382, 2011.

[6] E. L. Hahn. Spin echoes. *Phys. Rev.*, 80:580, 1950.

[7] Howard M. Wiseman and Gerard J. Milburn. *Quantum Measurement and Control*. Cambridge University Press, 2010.

[8] G. Waldherr, J. Beck, P. Neumann, R. S. Said, M. Nitsche, M. L. Markham, D. J. Twitchen, J. Twamley, F. Jelezko, and J. Wrachtrup. High-dynamic-range magnetometry with a single nuclear spin in diamon. *Nature Nanotechnology*, 7:105–108, 2012. doi: 10.1038/nnano.2011.224.

[9] N. M. Nusran, M. Ummal, and M.V Gurudev Dutt. High dynamic range magnetometry with a single electronic spin in diamon. *Nature Nanotechnology*, 7:109, 2012. doi: 10.1038/nnano.2011.225.

[10] Alexandr Sergeevich, Anushya Chandran, Joshua Combes, Stephen D. Bartlett, and Howard M. Wiseman. Characterization of a qubit hamiltonian using adaptive measurements in a fixed basis. *Phys. Rev. A*, 84:052315, Nov 2011. doi:10.1103/PhysRevA.84.052315. URL `http://link.aps.org/doi/10.1103/PhysRevA.84.052315`.

[11] J. P. Kestner, Xin Wang, Lev S. Bishop, Edwin Barnes, and S. Das Sarma. Noise-resistant control for a spin qubit array. *Phys. Rev. Lett.*, 110:140502, Apr 2013. doi: 10.1103/PhysRevLett.110.140502. URL `http://link.aps.org/doi/10.1103/PhysRevLett.110.140502`.

[12] J. R. Petta, A. C. Johnson, J. M. Taylor, E. A. Laird, A. Yacoby, M. D. Lukin, C. M. Marcus, M. P. Hanson, and A. C. Gossard. Coherent manipulation of coupled electron spins in semiconductor quantum dots. *Science*, 309:2180, 2005.

[13] B. M. Maune, M. G. Borselli, B. Huang, T. D. Ladd, P. W. Deelman, K. S. Holabird, A. A. Kiselev, I. Alvarado-Rodriguez, R. S. Ross, A. E. Schmitz, M. Sokolich, C. A. Watson, M. F. Gyure, and A. T. Hunter. Coherent singlet-triplet oscillations in a silicon-based double quantum dot. *Nature*, 481:344–347, 2011. doi:10.1038/nature10707.

[14] O. E. Dial, M. D. Shulman, S. P. Harvey, H. Bluhm, V. Umansky, and A. Yacoby. Charge noise spectroscopy using coherent exchange oscillations in a singlet-triplet qubit. *Phys. Rev. Lett.*, 110:146804, Apr 2013. doi: 10.1103/PhysRevLett.110.146804. URL `http://link.aps.org/doi/10.1103/PhysRevLett.110.146804`.

[15] M. D. Shulman, O. E. Dial, S. P. Harvey, H. Bluhm, V. Umansky, and A. Yacoby. Demonstration of entanglement of electrostatically coupled singlet-triplet qubits. *Science*, 336:202, 2012. doi:10.1126/science.1217692.

[16] C. Barthel, D. J. Reilly, C. M. Marcus, M. P. Hanson, and A. C. Gossard. Rapid single-shot measurement of a singlet-triplet qubit. *Phys. Rev. Lett.*, 103:160503, 2009.

[17] D. J. Reilly, C. M. Marcus, M. P. Hanson, and A. C. Gossard. Fast single-charge sensing with a RF quantum point contact. *Appl. Phys. Lett.*, 91:162101, 2007.

[18] S. Foletti, H. Bluhm, D. Mahalu, V. Umansky, and A. Yacoby. Universal quantum control in two-electron spin quantum bits using dynamic nuclear polarization. *Nature Physics*, 5:903, 2009.

[19] H. Bluhm, S. Foletti, I. Neder, M. S. Rudner, D. Mahalu, V. Umansky, and A. Yacoby. Dephasing time of GaAs electron-spin qubits coupled to a nuclear bath exceeding 200 μs. *Nature Physics*, 7:109, 2011. doi:DOI: 10.1038/NPHYS1856.

[20] W. A. Coish and D. Loss. Hyperfine interaction in a quantum dot: Non-markovian electron spin dynamics. *Phys. Rev. B*, 70:195340, 2004.

[21] D. Klauser, W. A. Coish, and D. Loss. Nuclear spin state narrowing via gate-controlled Rabi oscillations in a double quantum dot. *Phys. Rev. B*, 73:205302, 2006.

[22] C. Ferrie, C. E. Granade, and D. G. Cory. How to best sample a periodic probability distribution, or on the accuracy of hamiltonian finding strategies. *Quantum Information Processing*, 12:611, 2013.

[23] M. D. Schroer and J. R. Petta. Quantum dots: time to get the nukes out. *Nature Physics.*, 4:1745, 2008. doi: 10.1038/nphys1007.

Supplemental Material for "Suppressing qubit dephasing using real-time Hamiltonian estimation"

M. D. Shulman,[1] S. P. Harvey,[1] J. M. Nichol,[1] S. D. Bartlett,[2] A. C. Doherty,[2] V. Umansky,[3] and A. Yacoby[1]

[1] *Department of Physics, Harvard University, Cambridge, MA, 02138, USA*
[2] *Centre for Engineered Quantum Systems, School of Physics, The University of Sydney, Sydney, NSW 2006, Australia*
[3] *Braun Center for Submicron Research, Department of Condensed Matter Physics, Weizmann Institute of Science, Rehovot 76100 Israel*

(Dated: May 5, 2014)

SINGLESHOT SENSOR RESPONSE

In order to effectively sample ΔB_z oscillations without having to measure each evolution time t_k more than once, we rely on high fidelity readout, which is based on standard RF-reflectometry techniques[16,17]. The readout fidelity is routinely better than 0.98. Though the Bayesian estimate of ΔB_z has parameters to account for readout error (see below), it nevertheless requires that this error be small. Moreover, in order to effectively process and compare data with both the FPGA and with software rescaling, we must achieve high fidelity readout with both the data acquisition card (DAQ) and with the FPGA. Fig. S1**a** shows histograms of all of the measured values. The double-peaked structure indicates that, indeed, high fidelity readout is achieved with both the DAQ and the FPGA. The difference in the heights of the two peaks is caused by residual exchange (J) during evolution, which causes the axis of evolution around the Bloch sphere to be non-orthogonal to the initial state (see section). For the Bayesian estimate, which requires discretized data ($r_k = \pm 1$), we choose a threshold corresponding to the minimum between the peaks for the adaptive control on the FPGA.

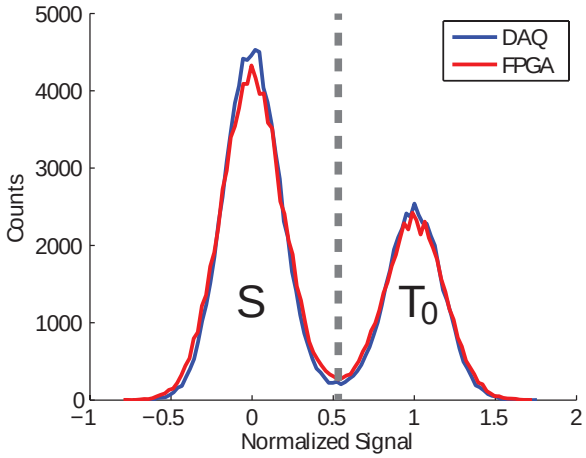

FIG. 1. **a**. A histogram of values measured by the data acquisition card (DAQ) and the FPGA/CDS show nearly identical double peaked structures, indicating that they are capable of consistent singleshot readout. The dashed line is chosen as the threshold for estimating ΔB_z with the FPGA.

FPGA AND EXPERIMENTAL APPARATUS

The reflected readout drive signal returns to room temperature through a cryogenic circulator and amplifier at 4K. The signal is amplified again at room temperature before being demodulated to DC. This DC signal is split and sent to a digitizing card (AlazarTech 660) in a computer and a home built correlated double sampler (CDS). The CDS digitizes the signal and performs a local reference subtraction to reject low frequency noise. The resulting 16 bit signal is converted to a low voltage digital signal and sent to the FPGA for processing. The FPGA is a National Instruments model PXI-7841R and is clocked at 40MHz to maximize processing speed. The probability $P(\Delta B_z|m_k)$ is computed for 256 consecutive frequencies in the estimation bandwidth, $\mathcal{B}$, in two parallel processes on the FPGA to decrease calculation time. Since $\mathcal{B} \approx$ 40MHz is larger than the residual fluctuations of ΔB_z, we increase the frequency resolution by computing the Bayesian estimate of ΔB_z for the the middle 256 frequencies inside of $\mathcal{B}$. For these parameters, the minimum calculation time is 3.7μs for a single t_k. The probability distributions are stored and updated as single-precision floating-point numbers, since we find that single-precision improves the accuracy of the estimator over fixed-point numbers.

After estimating ΔB_z, the FPGA returns the index (an integer between 1 and 256) of the most probable frequency, which must be converted to a voltage to control the VCO. To do so, we apply a linear transformation to the index, $V = G \times index + O$, where the O controls the detuning of the driving frequency. We tune the G to maximize T_2^* using adaptive control (Fig. S2**a**).

BAYESIAN ESTIMATE

We wish to calculate the probability that the nuclear magnetic field gradient has a certain value, ΔB_z, given a particular measurement record comprising N measure-

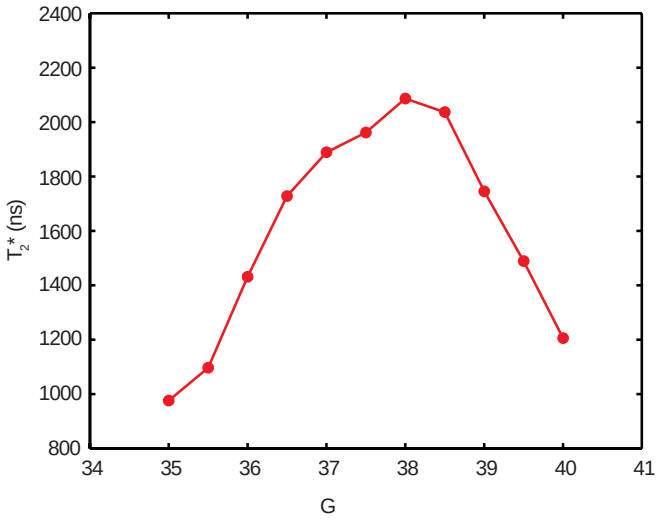

FIG. 2. **a**. T_2^* changes with the gain, G, converting a frequency index into a control voltage for the VCO. This allows for the optimal gain to be found.

ments. We follow the technique in Sergeevich *et. al.*[10] with slight modifications. Writing the outcome of the k^{th} measurement as m_k, we write this probability distribution as

$$P\left(\Delta B_z|m_N, m_{N-1}, ...m_1\right). \tag{1}$$

To arrive at an expression for this distribution, we will write down a model for the dynamics of the system, i.e. $P\left(m_N, m_{N-1}, ...m_1|\Delta B_z\right)$. Using Bayes' rule we can relate the two equations as

$$P\left(\Delta B_z|m_N, m_{N-1}, ...m_1\right) \cdot P\left(m_N, m_{N-1}, ...m_1\right) \tag{2}$$
$$= P\left(m_N, m_{N-1}, ...m_1|\Delta B_z\right) \cdot P\left(\Delta B_z\right). \tag{3}$$

First, we seek a model that can quantify $P\left(m_N, m_{N-1}, ...m_1|\Delta B_z\right)$ that accounts for realistic errors in the system, namely measurement error, imperfect state preparation, and error in the axis of rotation around the Bloch sphere. For simplicity, we begin with a model that accounts only for measurment error. Denoting the error associated with measuring a $|S\rangle$ ($|T_0\rangle$) as η_S (η_T), we write

$$P\left(S|\Delta B_z\right) =$$
$$\left(1-\eta_S\right)\cos^2\left(2\pi\Delta B_z t_k/2\right) + \eta_T \sin^2\left(2\pi\Delta B_z t_k/2\right) \tag{4}$$
$$P\left(T_0|\Delta B_z\right) =$$
$$\left(1-\eta_T\right)\sin^2\left(2\pi\Delta B_z t_k/2\right) + \eta_S \cos^2\left(2\pi\Delta B_z t_k/2\right) \tag{5}$$

We combine these two equations and write

$$P\left(m_k|\Delta B_z\right) = \frac{1}{2}\left[1 + r_k\left(\alpha + \beta\cos\left(2\pi\Delta B_z t_k\right)\right)\right] \tag{6}$$

where r_k=1 (-1) for $m_k = |S\rangle(|T_0\rangle)$ and α and β are given by

$$\alpha = \left(\eta_T - \eta_S\right), \quad \beta = \left(1 - \eta_S - \eta_T\right). \tag{7}$$

Next, we generalize the model to include the effects of imperfect state preparation, and the presence of nonzero J during evolution, which renders the initial state non-orthogonal to the axis of rotation around the Bloch sphere (see above). We assume that the angle of rotation around the Bloch sphere lies somewhere in the x-z plane and makes an angle θ with the z-axis. We define $\delta = \cos^2(\theta)$. Next, we include imperfect state preparation by writing the density matrix $\rho_{init} = (1-\epsilon)\left|S\right\rangle\left\langle S\right| + \epsilon\left|T_0\right\rangle\left\langle T_0\right|$. With this in hand, we can write down the model

$$P\left(S|\Delta B_z\right) = \eta_T + \frac{1}{2}(1 - \eta_S - \eta_T) \times$$
$$\left\{1 + (1-2\epsilon)\left[\delta + (1-\delta)\cos\left(2\pi\Delta B_z t_k\right)\right]\right\}, \tag{8}$$

$$P\left(T_0|\Delta B_z\right) = \eta_S + \frac{1}{2}(1 - \eta_S - \eta_T) \times$$
$$\left\{1 - (1-2\epsilon)\left[\delta + (1-\delta)\cos\left(2\pi\Delta B_z t_k\right)\right]\right\}. \tag{9}$$

Using the same notation for r_k=1 (-1) for $m_k = |S\rangle(|T_0\rangle)$, we rewrite this in one equation as

$$P\left(m_k|\Delta B_z\right) = \frac{1}{2}\left[1 + r_k\left(\alpha + \beta\cos\left(2\pi\Delta B_z t_k\right)\right)\right], \tag{10}$$

where we now have

$$\alpha = \eta_T - \eta_S + (1 - \eta_S - \eta_T)(\delta - 2\epsilon\delta) \tag{11}$$
$$\beta = (1 - \eta_S - \eta_T)(1-\delta)(1-2\epsilon). \tag{12}$$

We find the best performance for $\alpha = 0.25$ and $\beta = 0.67$, which is consistent with known values for qubit errors.

We next turn our attention to implementing Bayes' rule to turn this model into a probability distribution for ΔB_z. First, we assume that all measurements are independent, allowing us to write

$$P\left(\Delta B_z|m_N, m_{N-1}, ...m_1\right) = P\left(\Delta B_z|m_N\right) \cdot P\left(\Delta B_z|m_{N-1}, ...m_1\right)$$
$$= \prod_{k=1}^{N} P\left(\Delta B_z|m_k\right). \tag{13}$$

We next use Bayes rule (3) and rewrite this equation as

$$P\left(\Delta B_z|m_N, m_{N-1}, ...m_1\right) = \prod_{k=1}^{N} P\left(m_k|\Delta B_z\right)\frac{P(\Delta B_z)}{P(m_k)}. \tag{14}$$

Using our model (10) we can rewrite this as

$$P\left(\Delta B_z|m_N, m_{N-1}, ...m_1\right) = \tag{15}$$
$$\mathcal{N} P_0(\Delta B_z) \prod_{k=1}^{N}\left[1 + r_k\left(\alpha + \beta\cos\left(2\pi\Delta B_z t_k\right)\right)\right], \tag{16}$$

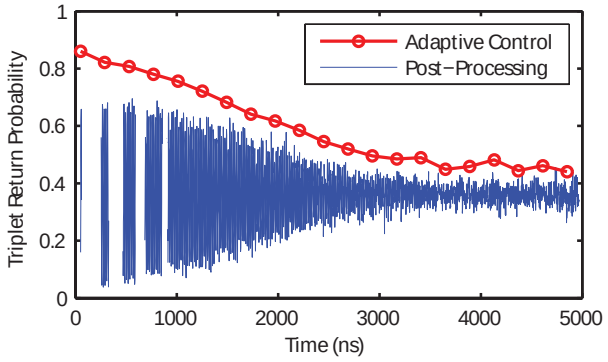

FIG. 3. **a**. When using the same estimation sequence, post-processed oscillations (blue) and data taken using adaptive control (red) show the same decay, indicating similar performance of the estimation. The post-processing technique allows us to explore estimation sequences that are too fast for the FPGA.

where $\mathcal{N}$ is a normalization constant, and $P_0(\Delta B_z)$ is a prior distribution for ΔB_z which we take to be a constant over the estimation bandwidth, and to which the estimator is empirically insensitive. With this formula, it is simple to see that the posterior distribution for ΔB_z can be updated in real time with each successive measurement. After the N^{th} measurement, we choose the value for ΔB_z which maximizes the posterior distribution (16).

SIMULATION WITH DIFFUSION

We simulate the performance of our software scaling and hardware (FPGA) estimates of ΔB_z using the measured value of the diffusion rate. We assume that ΔB_z obeys a random walk, but assume that during a single evolution time t_k, ΔB_z is static. This assumption is valid $\sqrt{t_N \mathcal{D}} T_2^* \ll 1$, where $\mathcal{D}$ is the diffusion rate of ΔB_z. For an estimation of ΔB_z with N different measurements, we generate a random walk of N different values for ΔB_z (using the measured diffusion), simulate the outcome of each measurement, and compute the Bayesian estimate of ΔB_z using the simulated outcomes. By repeating this procedure 4096 times, and using the mean squared error, $\text{MSE} = \langle \left(\Delta B_z - \Delta B_z^{\,estimated}\right)^2 \rangle$ as a metric for performance, we can find the optimal number of measurements to perform. To include the entire error budget of the FPGA apparatus, we add to this MSE the error from the phase noise of the VCO, the measured voltage noise on the analog output controlling the VCO, and the diffusion of ΔB_z during the "operation" period of the experiment.

SOFTWARE POST PROCESSING

The estimate of ΔB_z can be independently verified using software analysis. In this experiment, we use the same method to estimate ΔB_z as in the adaptive control experiment, but in the operation segment perform oscillations around ΔB_z for verification. We choose m different evolution times and measure each n times for a total of $N_{tot} = m \times n$ measurements of ΔB_z. In the i^{th} experiment ($i = 1, 2, \ldots N_{tot}$), we evolve for a time $t_{evo,i}$, accumulating phase $\phi_i = \Delta B_{z,i} t_{evo,i}$. Because we make a precise measurement of ΔB_z at the start of each experiment, we can employ it to rescale the time, $t_{evo,i}$, so that the phase accumulated for a given time is constant using the equation,

$$\tau_i \equiv t_{evo,i} \frac{\Delta B_{z,i}}{\langle \Delta B_z \rangle}$$

This sets $\phi_i(\tau_i) = \langle \Delta B_z \rangle \tau_i$, with residual error arising from inaccuracy in the estimate of $\Delta B_{z,i}$. The data are then sorted by τ, and points of similar τ are averaged using a Gaussian window with $\sigma_\tau = 0.5$ ns $\ll T \approx 16$ ns, where T is the period of the oscillations.

To compare post-processing with adaptive control, we first perform the same estimation sequence for both software post-processing and adaptive control, with a 250 kHz repetition rate, $t_{samp} = 12$ ns and N =120, followed by an operation sequence of 30 measurements. We find $T_2^* = 2148 \pm 30$ ns with software and $T_2^* = 2066$ ns with adaptive control, showing good agreement between the two approaches (Fig. S3**a**).

For the software post-processing, we can reduce the amount of diffusion that occurs during the operation sequence by performing only one verification measurement following the same estimation sequence, enhancing T_2^*, to 2580 ± 40 ns. For the software rescaling in Fig. 4d, the 109 estimations were performed in 225 μs instead of the 440 μs used by the FPGA, yielding $T_2^* = 2840 \pm 30$ ns. This is likely limited by diffusion and the precision of the estimator with N=109.